DESIGNING ADVANCED BIOINKS FOR 3D PRINTING COMPLEX TISSUE STRUCTURES

A Thesis

by

SCOTT ANDREW WILSON

Submitted to the Office of Graduate and Professional Studies of
Texas A&M University
in partial fulfillment of the requirements for the degree of

MASTER OF SCIENCE

Chair of Committee,	Akhilesh Gaharwar
Committee Members,	Roland Kaunas
	Arum Han
Head of Department,	Anthony Guiseppi-Elie

August 2017

Major Subject: Biomedical Engineering

ABSTRACT

Three-dimensional (3D) printing is an emerging approach for rapid fabrication of complex tissue structures using cell-loaded bioinks. However, 3D bioprinting has hit a bottleneck in progress due to the lack of suitable bioinks that are printable, have high shape fidelity, and are mechanically resilient. In this study, we introduce a novel family of nanoengineered bioinks consisting of Kappa-Carrageenan (κCA) and nanosilicates (nSi). κCA is a biocompatible linear sulfated polysaccharide derived from red algae and is able to undergo quick thermoreversible and ionic gelation. The shear-thinning characteristics of κCA was modified by nanosilicates to develop a printable bioink. By tuning κCA-nanosilicate ratios, the thermoreversible gelation of the bioink can be controlled to obtain high shape retention. The unique aspect of the nanoengineered κCA-nSi bioink is its ability to print closer to physiologically relevant scale tissue constructs than conventional bioinks without requiring secondary supports. We envision that nanoengineered κCA-nSi bioinks can be used to bioprint complex, large-scale, cell-laden tissue constructs with high structural fidelity and mechanical stiffness for applications in custom bioprinted scaffolds and tissue engineered implants.

NOMENCLATURE

ECM	Extracellular Matrix
G’	Storage Modulus
G’’	Loss Modulus
GelMA	Gelatin Methacrylate
HA	Hyaluronic Acid
IPNs	Interpenetrating Networks
K^+	Potassium
κCA	Kappa-Carrageenan
nSi	Nanosilicates or Laponite XLS
PEO/G	Poly(ethylene oxide/glycol)
RGD	Arginyl-glycyl-aspartic acid
XLG	Laponite XLG

CONTRIBUTORS AND FUNDING SOURCES

Contributors

This work was supported by a thesis committee consisting of Professor Gaharwar (advisor) and Professor Kaunas of the Department of Biomedical Engineering and Professor Han of the Department of Electrical and Computer Engineering.

All work conducted for the thesis was completed by the student under advisement of Professor Gaharwar.

Funding Sources

This work was made possible by the NIH under Grant Number NIH R03 EB023454.

TABLE OF CONTENTS

Page

LIST OF FIGURES

Page

CHAPTER I

INTRODUCTION AND LITERATURE REVIEW

Shear-thinning hydrogels are promising candidates for 3D bioprinting due to their non-Newtonian behavior and stress-relaxation properties.[1] Hydrogel-based bioinks have been used to print cells in complex patterns for biomedical applications due to their biocompatibility and ability to recapitulate extracellular matrix (ECM).[2] Some of the most commonly used polymers in bioprinting include alginate[3, 4], gelatin methacrylate (GelMA)[5, 6], poly(ethylene oxide/glycol) (PEO/G)[7], hyaluronic acid (HA)[8], and agarose[9, 10]. Both alginate and agarose individually hold additional promise due to the high viscosities they can achieve, demonstrating high resiliency to the printing process.[9, 11] These and other highly viscous polymers are often incorporated in blended bioinks as they can increase the printability of more bioactive but less printable polymers, such as gelatin, GelMA, HA, and fibrinogen.[11-15] However, hydrogel-based bioinks still have limited shape fidelity after printing, low mechanical strength, and lack the ability to fabricate large scale and self-supporting tissue constructs.[16-21] To address this critical need, advance bioinks are designed as rapidly gelling, shear-thinning hydrogel composites; however, these bioinks often require support baths, photocrosslinking, or post processing that can add complexity to the print, lead to cell death, and produce mechanically weak constructs.[22, 23] Thus, there is critical need to develop new bioinks with shear-thinning characteristics, high print fidelity, tunable mechanical strength, high cell viability, and the ability to print anatomical-scale structures.

To address the aforementioned challenges, as well as broaden the current selection of bioinks we have developed a novel family of shear-thinning bioinks from Kappa-Carrageenan (κCA) and nanosilicates (nSi or Laponite XLS). κCA is a linear sulfated polysaccharide derived from red algae with alternating 3,6-anhydro-D-galactose and β-D-galactose-4-sulphate repetitive units (**Figure 1a**).[24] This natural polymer has previously shown to not only be biocompatible, but also a viscous aid that is able to undergo quick thermoreversible and ionic gelation, as well as a shear-thinning material at higher concentrations in solution.[25, 26] When κCA is heated and dissolved in water it presents a random coil structure; upon subsequent cooling, double helices (junctions) are formed due to hydrogen bonding between galactose units on the polymer backbone (**Figure 1b**).[27] This thermoreversible gelation can then be further stabilized by ionic crosslinking through positive ions, such as potassium (K^+), with κCA's negatively charged sulfate groups.[28] Compared to other positive ions, K^+ has shown to interact the most synergistically with κCA to produce strong gels.[28] κCA's properties are complemented with the inclusion of nSi. Laponite XLS is a negatively charged synthetic silicate that has shown to increase the mechanical properties and biocompatibility of hydrogels due to their large surface to volume ratio and charged nature.[29-31] These nSi have negatively charged surfaces, which allows for simple suspension in water at high concentrations without premature gelation. Additionally, this allows for enhanced control over printing since there are no positive charges to interact with the anionic κCA. By tuning the κCA-nSi bioinks' printing and material properties we were able to print anatomical-scale complex constructs with high resolutions and shape-fidelity (**Figure 1c**).

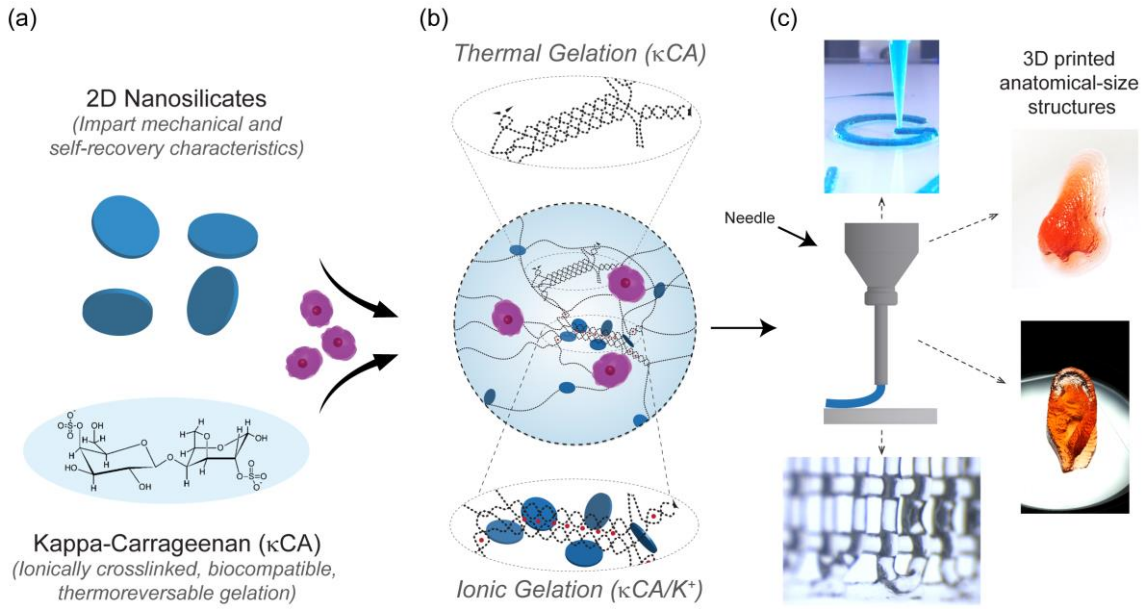

Figure 1. A broad overview of the bioink's components, mechanisms of crosslinking, and printing of complex structures. (a) A schematic representation of the bioink's components including κCA's molecular structure. (b) Schematic showing the dual crosslinking process of thermoreversible gelation then ionic gelation. (c) Images of complex structures including a letter G, nose, ear, and lattice network printed using the κCA-nSi bioink.

CHAPTER II

MATERIALS AND METHODS

Preparation of Kappa Carrageenan/Synthetic Nanosilicate Bioinks

Nanosilicates (Laponite XLS, BYK-Chemie GmbH, Wesel, Germany) were slowly added to 10 mL of diH2O and vigorously mixed using a magnetic stir rod and hot plate for 30 minutes until the initially opaque solution turned clear and nanosilicates were suspended in solution. For the initial bioinks, the nanosilicate suspensions were then heated to the desired temperature, 25ºC, 40ºC, or 60ºCto 80 °C and powdered Kappa-Carrageenan (κCA, Tokyo Chemical Industries, Japan) was slowing added and thoroughly mixed into the solutions for 30 additional minutes. After mixing was completed the solutions were brought down to the desired temperature, 60 or 40 °C.

For subsequent inks, including cell laden inks, this process was repeated with the inks mixed at 80 °C and then cooled to 40 °C in a vacuum oven. Using these processes κCA/XLS formations were created using different wt%'s for each component of the bioink. For all testing and printing, solutions were placed in a vacuum oven at the desired temperature (25 - 60 °C) and utilized when the temperature of the solution reached said desired temperature.

Printability Tests

Printability tests were performed by filling 3 mL syringes with bioinks at specified temperatures, then loaded onto a NE-1000 syringe pump (East Farmingdale, New York).

The syringes were fitted with a 23 gauge blunt tipped stainless steel needle (Jensen Global Inc, Santa Barbara, CA) and extruded with a 0.3 mL/hr flow rate. The pump-syringe apparatus was tilted 45º and extruded onto a glass slide.

3D Printing Process

A HYREL System 30M 3D printer (HYREL L.L.C., Norcross, GA) was used for printing all constructs. Ink compositions of 5 mL were loaded into a VOL-25 Extruder cartridge (HYREL L.L.C., Norcross, GA) at 40 °C. The extruder system was then connected to the printer and fitted with a 23 gauge blunt tipped stainless steel needle (Jensen Global Inc, Santa Barbara, CA). STL files were generated from 3D CAD drawings created in SOLIDWORKS and converted to G-code using Slic3r. G-Code files were then input into Hyrel's proprietary software (Repetrel) which controlled the printer and print parameters. Unless otherwise specified, prints were performed with the following parameters: print head speed 2 4 mm/s, nozzle height from print surface 325 350 μm, and a flow rate of 0.3 mL/hr. Constructs were printed onto glass slides and crosslinked with 5 wt% KCL (potassium chloride) for 5 minutes before being moved into a 10X PBS (Phosphate-buffered saline) solution. Constructs were dyed with food coloring and imaged using a stereomicroscope (SteREO Discovery.V8, Carl Zeiss Meditec AG, Oberkochen, Germany). Images were processed and analyzed in ImageJ to quantify fiber size.

Rheological Analysis

All rheological testing was performed with a stress controlled rheometer (DHR-2 Discovery Hybrid Rheometer, TA Instruments, New Castle, Delaware) using 40 mm

parallel plate geometry at a gap of 0.2 mm in conjunction with a solvent trap. All tests besides temperature sweeps were performed at 40 °C to replicate the temperature of the ink inside the cartridge while being printed. To evaluate recoverability of the material, oscillatory time sweeps (1 Hz) were performed in 60 second intervals at alternating 100% and 1% strains. Shear-thinning tests were run with a shear rate from .001 to 1000 s-1. To measure yield stress, oscillation stress sweeps were performed at 1 Hz from .01 to 1000 Pa. Finally, temperature sweeps were conducted from 60 °C to 20 °C at a frequency of 1 Hz and a stress of 10 Pa.

Mechanical Testing

To determine the modulus of the material, cyclic compression testing was performed with an ADMET eXpert 7600 Single Column Testing System (ADMET, Inc., Norwood, Massachusetts) fitted with a 25 lb load cell. Testing was implemented at 20% compression and a strain rate of 10 mm/min. After mixing, inks (80 °C) were poured into a glass petri dish and cooled to room temperature. These samples were punched out with a 7mm punch and placed into 5 wt% KCL (potassium chloride) for 5 minutes before being moved into a 10X PBS (Phosphate-buffered saline) solution for 1hr. The samples were then gently blotted to remove excess water and used for testing In vitro Studies.

Bioprinting

Cell laden inks were fabricated as previously stated, kept at 40 °C, and were composed of 2.5 wt% κCA and 6 wt% XLS. MC3T3-E1 mouse preosteoblasts (ATCC, Manassas, Virginia) were cultured in Dulbecco's modified eagles medium (DMEM,

Hyclone) supplemented with 10% fetal bovine serum (FBS, Atlanta Biologicals) and 1% penicillin/streptomycin (100U/100 µg/mL, Gibco). Once cells reached desired confluency, cells were passaged and resuspended in inks. Cell laden ink was loaded and printed as previously described onto glass slides. Constructs were then crosslinked by with KCL for 5 minutes, rinsed with 10X PBS, placed into 12 well plates with culture media, and incubated at 37 °C until further analysis.

Imaging

To visualize cells encapsulated within bioinks, cells were incubated at 37 °C with 2 µM Cell Tracker Red or Green Dye (TermoFisher) in 1X PBS for 30 minutes prior to passaging. Cell imaging was performed using a (Nikon, TE2000-S) fluorescent microscope at 3, 24, and 48 hours after encapsulation. Finally, an Alamar Blue assay was performed at 1,3, and 7 days to quantify cell metabolic activity within the printed structures over time. Metabolic activity was normalized to cells seeded on tissue culture plastic.

CHAPTER III

RESULTS AND DISCUSSION

Designing κCA-Nanosilicate Bioink Formulations

A key characteristic of bioinks is the ability of the material to be continuously extruded using a printing needle. To design bioinks, we first evaluated the printability of κCA and κCA/nSi nanocomposites by using an extrusion test. The extrusion tests were performed by pouring κCA and κCA-nSi solutions into syringes and extruding using a syringe pump (**Figure 2a**). If the material could be continuously extruded without premature gelation and with minimal spreading after extrusion, it was deemed extrudable. We investigated the effect of κCA (1-4 wt%) and nSi (0-6 wt%) concentrations on the ability of the gel to be extruded. The lower concentrations (1-1.5 wt%) of κCA were low-viscosity fluids and were not able to retain an extruded shape at 40 °C. This might be due to high polymer chain mobility at low κCA concentrations that may prevent gelation due to limited chain interactions. With an increase in κCA concentration, it is expected to reach a critical solution concentration that results in formation of viscous gel.

At a critical concentration, there will be enough galactose units interacting with other galactose units, on the polymer chains, that results in physically entangled network due hydrogen bonding between chains.[27] The observed low-viscosities were similar to previous work investigating the critical gelation point of κCA, with a critical gel concentration being calculated at 1.9 wt% κCA at 40°C.[32] From room temperature

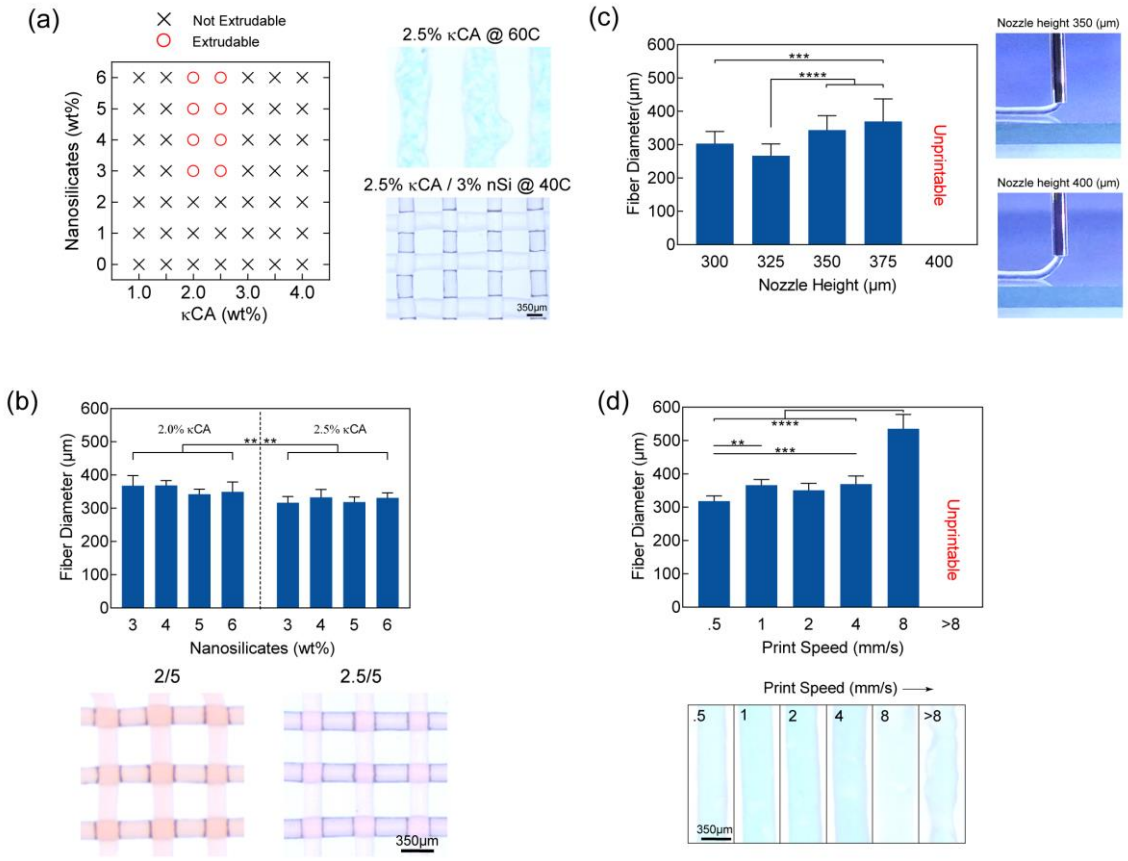

Figure 2. Optimizing material processing and printing parameters. (a) Graph representing the printability of pure κCA and κCA-nSi compositions. Corresponding images exhibit the differences that printing temperature and the addition of nSi have on the fiber diameter. (b) Composition groups previously identified in (a) reveal a significant difference in fiber diameter though both retain a high resolution. (c) The change in nozzle height effects the size of fiber diameter. (d) Print speed tests reveal the material can be printed at a variety of speeds with 8mm/s and above being too fast for high resolution fibers.

observations, higher concentrations (2-4 wt%) of κCA were highly viscous solutions. To disrupt hydrogen bonding the solutions must be heated to 60°C for extrusion. Upon extrusion of 2-4 wt% κCA, shape retention was low and a high amount of spreading was observed. With time the solution regained its viscosity however it is difficult for 3D printing. While the extrusion bed temperature could be controlled to allow for faster

gelation of κCA, tight temperature controls are necessary for cell bioprinting. Based on extrusion test, we selected 2 and 2.5 wt% κCA as printable formulations.

The compositions of 2 and 2.5 wt% κCA with 3-6 wt% nSi had good shape retention and did not undergo premature gelation. This might be due to the addition of nSi that allows additional sites for hydrogen bonding with the polymer backbone; which imparts shape retention, but also disrupts the polymer-polymer interactions of κCA to thermoreversibly gel even at high concentrations. Based on these extrusion results, 2 and 2.5 wt% κCA were chosen as optimal polymer concentrations when used with 3-6 wt% nSi for 3D printing. The improvement in printability of κCA with the addition of nSi can been seen in shape-retention of the extruded filament using the bioprinter (**Figure 2a**). Shape retention elucidates if a material can be printed while optimization of resolution, print fidelity, and shape retention after 3D printing can determine the applications in which the material can be used.

To mimic native tissue architecture using 3D microextrusion printing, it is important to evaluate the resolution of the bioink. The control over printing parameters and material selection have significant effect on the resolution of printed constructs. Typical resolution of extruded fibers range from 150 μm to 1 mm.[33] We investigated the effect of κCA (2 and 2.5 wt%) and nSi (3, 4, 5, 6 wt%) concentration on printing resolution (**Figure 2b**). When using high viscosity shear-thinning materials, it has been observed that increasing polymer concentration can increase the printed resolution of the bioink.[4, 9, 15, 34] Increasing polymer concentration allows enhance polymer-polymer interactions to occur between polymer chains, which in turn can enable the bioink to have

greater shape retention after it is printed. We believe by increasing the concentration of κCA, we increased the amount of available interaction sites for hydrogen bonding between κCA polymer chains which led to an enhanced resolution. The resolution was further quantified, revealing the 2 and 2.5 wt% κCA group's average fiber diameters were significantly different (p-value < 0.0001) from each other; specifically, the 2.5 wt% κCA had a higher average resolution (325 ± 8.4 μm) than 2.0 wt% (357 ± 13.3 μm). As increasing the κCA concentration exhibited an increase in resolution, we continued to use the 2.5 wt% κCA and 6 wt% nSi formulation to optimize the printing parameters of the printing system.

Print speed and the nozzle to print bed height are two parameters that have been reported to influence printing resolution.[8, 35] If the nozzle is too far from the print bed or if the print speed is too high, this can result in inconsistent deposition of fibers. In addition, finding the closest print height that matches the height of the deposited fibers is imperative to fabricating large constructs without delamination of layers. With this said, the distance of the nozzle from the print platform was investigated and it was determined that a height of 350 μm allowed for the closest fiber diameter (343 ± 43 μm) relative to the needle size (337 μm) (**Figure 2c**). At a nozzle height of 400μm, the material was not able to be deposited on the print bed. Printing at this height gives us a high resolution and allows for close deposition of fibers as seen in **Figure 1c**. Additionally, print speed is important for cell survival; the less time taken to print can increase cell survival, especially when fabricating larger constructs (**Figure 2d**).[33] There is also a tradeoff between print speed and resolution; lower speeds can produce higher resolutions due to the material

having more time to gel. Above the highest speed of 8 mm/s, the bioink was unprintable, having an inconsistent fiber diameter. However, fiber resolution was still high (535 ± 43 μm) even at 8 mm/s speeds. For further testing we chose 4 mm/s as it had a higher resolution (369 ± 25 μm) than 8 mm/s while remaining faster for printing larger constructs. By optimizing the material selection and printing parameters of the bioink and bioprinter, we synthesized a bioink with high shape fidelity, resolution, and retention. We further evaluated bioink containing 2.5 wt% κCA with different nSi concentrations (4, 5, 6 wt%) to print complex structure.

κCA-Nanosilicate Interactions During 3D Printing

During printing, the κCA-nSi bioink is subjected to either a static or dynamic environment. (**Figure 3a**). Initially, κCA exhibits a random coil structure that becomes aligned and elongated under shear; then upon cooling, the material displays a double helix structure, that is further stabilized by ionic crosslinking.[27] κCA‘s material properties can be grouped into sol, shear-thinning, and gel behavioral during the printing process. From these regions, we explored the effect of nSi addition on κCAs’ ability to flow under shear force and recover from flow deformation.

Low viscosity materials can be used for printing but have the observable limitation of shape fidelity after printing, which necessitates the use of highly viscous materials that are shear-thinning.[23] One model that mathematically describes shear-thinning fluids is power-law rheology in which viscosity is raised to a flow index. Flow index describes a materials’ ability to thicken, thin, or remain Newtonian. A flow index of less than one

indicates a shear-thinning material, this can be observed with a noticeable decrease in viscosity when there is an increase in shear rate (**Figure 3b**).[36] κCA and κCA-nSi were observed to have similar shear-thinning characteristics, as quantified by the power law flow index numbers of 0.56, 0.57, 0.58, and 0.54 for 0 wt%, 4 wt%, 5 wt%, and 6 wt% nSi, respectively. These value could indicate that nSi had no strong effect on κCA's shear-thinning ability and did not significantly disrupt κCA's polymer junction's ability to align when subjected to continuous shear. Measurements of κCA's flow behavior index indicated κCA had a greater shear-thinning ability than commonly used polymers for bioink blends, such as alginate. Previous reports have indicated a flow behavior index of 0.90 for 2.25 wt% alginate compared to the observed 0.56 for κCA in the present study.[37, 38] This shear-thinning behavior indicates how the material will react in a dynamic environment which prefaces the final static environment the κCA-nSi bioink will experience after printing.

The effect of nSi on recovery was investigated by subjecting the bioink precursor solutions to low (1%) and high (100%) strain percentages. During the printing process the bioink is subjected to different degrees of strain before it is printed and must be deformable and able to reform many times while retaining its mechanical properties. In addition, percent recovery from strain is also an indication of shape retention after printing which can therefore effect the mechanical properties of the printed constructs. It was observed that κCA's storage modulus (G') significantly decreased, from 360 ± 15 Pa to 249 ± 15 Pa, when subjected to alternating high (100%) and low (1%) strains, presenting a low percent recovery of its G' (69%) (**Figure 3c**). Importantly, all the nSi compositions

exhibited high percent recovery of *G'*, with 6 wt% nSi having a percent recovery of 99%. Upon examination of the *G'* value for κCA, we believe the secondary intermolecular bonds between polymer chains were unable to fully reform after subjection to multiple cycles of high strain. Alternatively, the addition of nSi resulted in fast reversible interactions between polymer and nanoparticles. This could be due to the nSi's interacting with κCA through hydrogen bonding. This is important for bioprinting since constructs are not fabricated using continuous extrusions; instead, bioinks are either quickly extruded and subject to shear or held at rest, depending if material deposition is required or not. Though bioink loaded with nSi had lower *G'*s than κCA alone, recoverability of mechanical characteristics is a more appropriate measure of the material behavior in relation to a dynamic printing environment. It is possible, that pure κCA had greater hydrogen bonding potential than nSi compositions though polymer-polymer interactions that were disrupted by polymer-nanosilicates interactions.

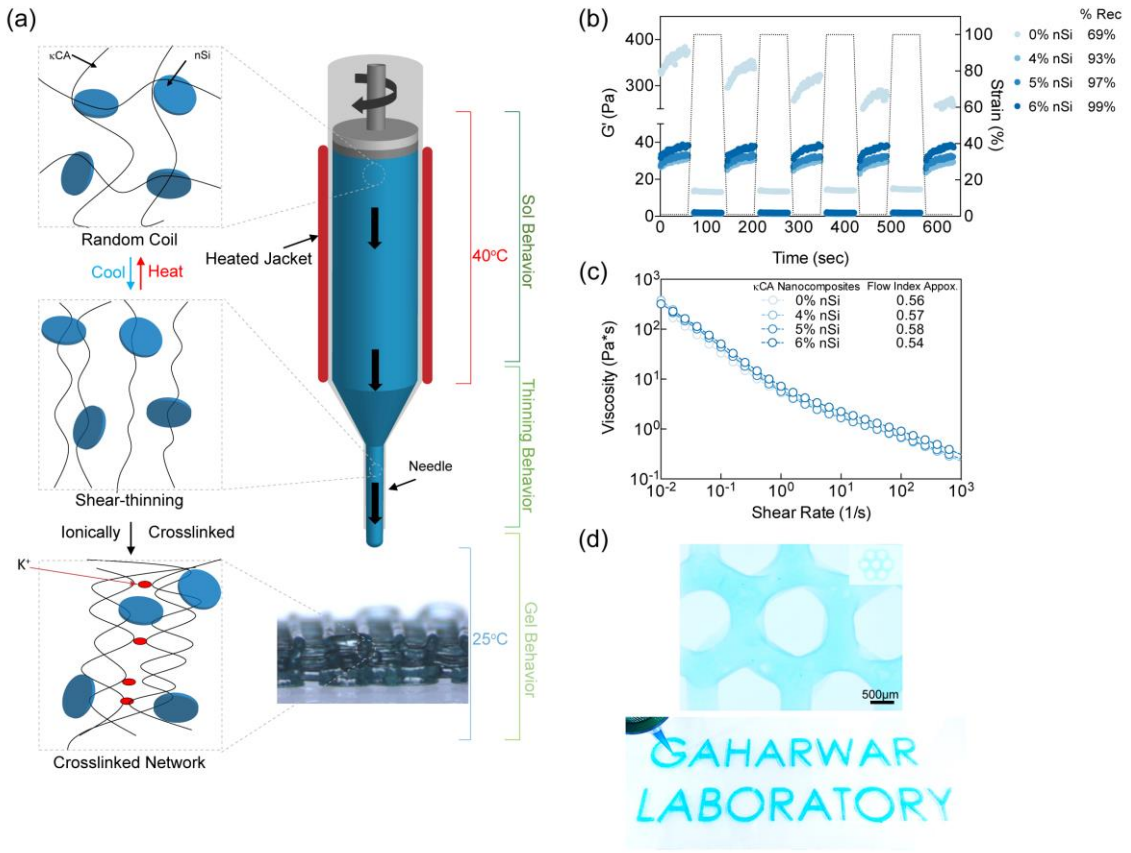

Figure 3. A schematic of κCA's coil-to-helix transition and material properties during the printing process. (a) κCA undergoes thermoreversible gelation upon heating and cooling which results in the formation of double helical structures that can then be ionically crosslinked with the introduction of K+ ions to form a stable network. (b) Time sweep at 40°C demonstrating percent recovery of bioink's storage modulus with the introduction of nSi. (c) Shear rate sweep revealing the shear-thinning nature of κCA and κCA-nSi bioinks. (d) Due to the bioink's high percent recovery (b) and shear-thinning characteristics (c), complex structures can be printed.

Yield Stress and Temperature Characterization

Investigation into yield stress is an important parameter for 3D printing as it describes the minimum stress needed for materials to flow. Rheology is a powerful platform to analyze the flow properties of a material, especially, the properties of a bioink. κCA forms random coil due to hydrogen bonding between galactose units when at rest as

it reduces the free energy within the structure. When subjected to a low stress environment analogous to (being held in the barrel without extrusion) κCA polymer chains remain in a random coil configuration. With increasing stress beyond the linear viscoelastic region (LVR), crossover of *G'* and *G''* was observed indicating network yielding. The yield stress point (also known as crossover point) is reached when the applied shear stress exceeds the attractive force caused by secondary intermolecular bonds (such as hydrogen bond) within the physically crosslinked network. The effect of nanosilicates on yield stress of bioinks were determined using shear stress sweep. κCA had a yield stress of 33±1 Pa, while addition of 6% nSi reduced the yield stress to 4.2 ± 0.76 Pa (**Figure 4a**). This yield stress indicates the force needed to allow the material to flow. In pure κCA solutions the hydrogen bonds between polymer strands and junctions are strong, which is reflected in the higher yield stress. However, the addition of nanosilicates result in lower yield stress due to its ability to disrupt polymer-polymer entanglement and improve reversible physical interactions between polymer–nanosilicate.

Amplitude stress sweeps determine yield stress under isothermal conditions (40°C). However above the gelation temperature, κCA polymer chains are in a random coil conformation that changes to a double helix conformation when the temperature is lowered below the gelation point. These double helices are stabilized by hydrogen bonding between anhydrous galactose units in the κCA polymer chain. In this study's printing set-up, the material was printed at 35-40°C onto a 25°C print bed. For a successful print to occur, the bioink should not thermoreversibly gel at or close to 37°C. To simulate this and evaluate the effect of nSi addition on the gelation temperature of the bioink compositions,

temperature sweeps were performed from 60°C to 20°C (**Figure 4b**). Pure κCA gelled close to 40 °C which translated to an unprintable material (**Figure 4c**). However, nSi compositions had significantly lower gelation temperature, around 35°C, which exhibited high shape retention when 3D printing. We believe that the addition of nSi disrupts the hydrogen bonding between κCA polymer chains which allows the double helices to form, lowering the gelation point of the material. This disruption could stem from the nSi potential to form hydrogen bonds with κCA, taking away some of the κCA polymer chains ability to interact with itself.[39-41] From this and previously shown data we chose the 6 wt% nSi composition for further 3D printing, due to its ability to have high printability, shape-fidelity, and physiologically relevant gelation temperature.

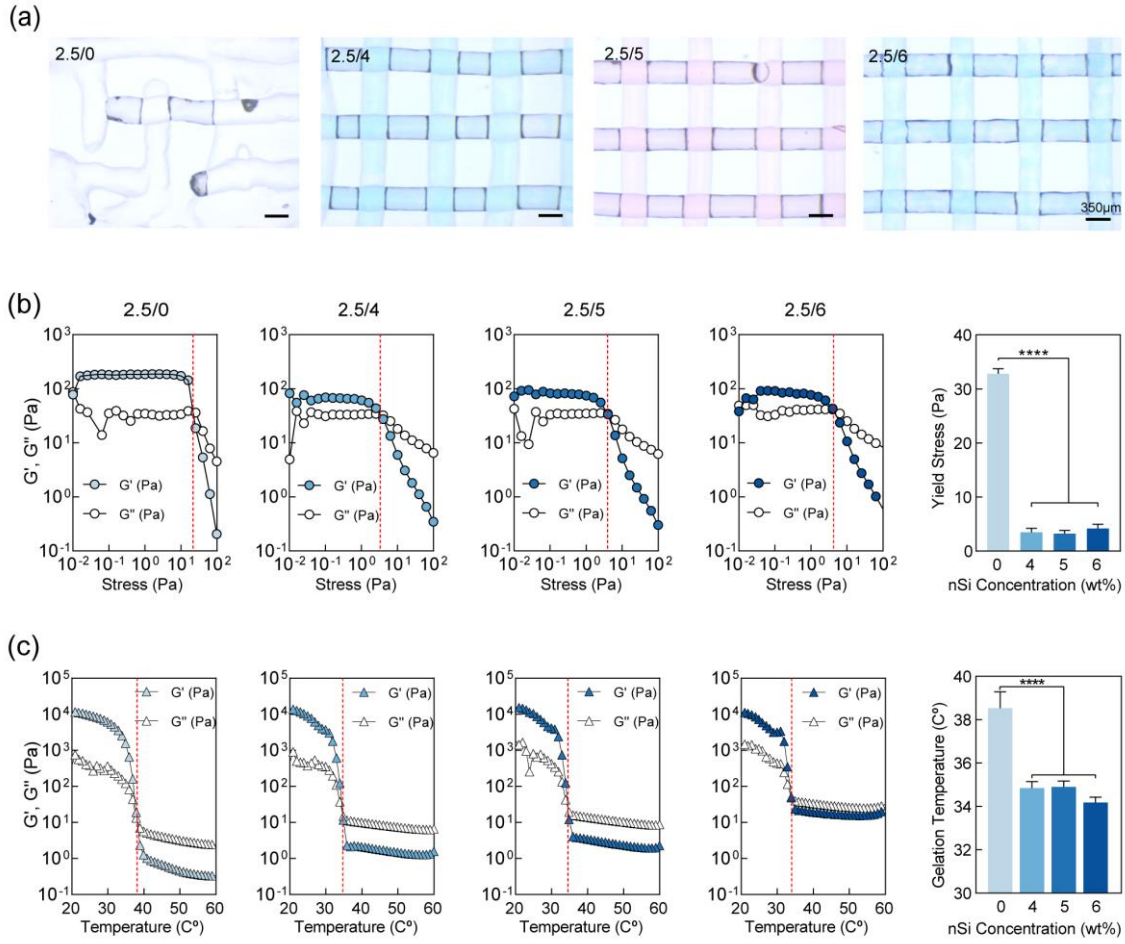

Figure 4: Rheological analysis of κCA-nSi bioinks. (crossover point = dashed red line)
(a) Pure κCA could not be printed but the addition of nSi allowed printing with high shape fidelity and resolution. (b) Stress sweeps showing storage (G') and loss modulus (G'') crossover points (yield stress). Yield stress quantification from stress sweeps reveals a significant decrease in yield stress from κCA bioink compared to κCA-nSi compositions. (c) Temperature sweeps starting at 60°C and cooled to 20°C show crossover point (gelation point) of bioink compositions. Gelation point analysis shows that in the physiological viable temperature range of 37°C to 40°C, κCA on its own cannot be printed due to premature gelation. The addition of nSi allows those compositions to be printed at 37°C and above.

3D Printing of Complex Constructs

One of the primary goals of 3D bioprinting is to print a complex organ or organ systems.[42, 43] However, current bioinks lack mechanical strength as well as printability to print larger, meso-scale architectures. To demonstrate the κCA-nSi bioinks ability to print complex shapes with high shape-fidelity, we printed a variety of constructs (**Figure 5**). Numerous lattice structures were printed to showcase the shape fidelity and high resolution of the 2.5% κCA- 6%nSi bioink (**Figure 5a**). Large as well as small lattice can be printed without compromising lattice porosity. The κCA-nSi bioinks has the ability to print large over hangs and support multiple layers. To mimic more complex architectures, a bioink must be able to print with rounded edges; this was observed by printing high aspect ratio cylinder (**Figure 5b**). This printed cylinder reveals high shape retention, even under the load of many successive layers (~30 layers), which is difficult to achieve using softer bioinks. The high stiffness of κCA-nSi bioink and rapid thermoreversible gelation allowed multilayered constructs to be printed without collapsing. Importantly, this renders a stable structure that can then be ionically crosslinked without the need for added complexity of support baths or UV radiation. The κCA-nSi bioinks can also print self-supporting anatomical-size structures such as nose, and ear (**Figure 5c**).

After printing, the structure can be crosslinked using potassium ions (K^+) to obtain mechanically resilient structure. We evaluated the effect of nanosilicate addition to κCA on mechanical properties of crosslinked nanocomposites using uniaxial compression. Nanocomposite gels were fabricated using molds and after ionic crosslinking with K^+. There was a significant increase in the mechanical properties of the hydrogels due to

nanosilicate addition (**Figure 5d**). Compressive modulus for pure 2.5wt% κCA gels was 85±5.7 kPa, while the addition of 6 wt% of nSi resulted in almost 2.5-fold increase to 208±6.5 kPa. The mechanical properties of κCA-nSi hydrogels are similar to some of the tissues that are subjected to mechanical stress such as cartilage and blood vessels. To our knowledge available bioink lack sufficient mechanical strength and are not able to match the physiologically-relevant mechanical stiffness. To demonstrate this aspect, we identified and compared modulus of available bioinks with κCA-nSi formulations (**Figure 5e**). Specifically, we compared three major classifications of bioinks: single polymer, polymer blends, and nanocomposites. Single polymer bioinks include agarose[9, 10], alginate[3, 4], GelMA[5, 6], and PEG-DA[7]; polymer blends consist of alginate/chitosan[44], GelMa/Gellan Gum[14], alginate/GelMA[15], alginate/GelMA/PEGTA[11], and GelMA/silk.MeOH[45]; and nanocomposite consist of alginate/hydroxyapatite(nHAp)[46], GelMa/gold nanoparticles (GNP) and nanocellulose(NFC)/alginate[34, 47]. The κCA-nSi bioink had a higher modulus (208 ± 6.5 kPa) than all the presented bioinks, apart from PEGDMA mixed with bioactive glass and hydroxyapatite (22 wt% total); an interesting result considering many bioinks were covalently crosslinked. There was not a noticeable difference between bioinks with one polymer compared to blends, though nanocomposites did appear to be the strongest group. The κCA-nSi bioink has a definite advantage in terms of mechanical characteristics when considering it is in the middle of the range of bioinks for overall polymer weight percentage and is only physically crosslinked. This comparison shows the bioinks strength and uniqueness as a novel bioink.

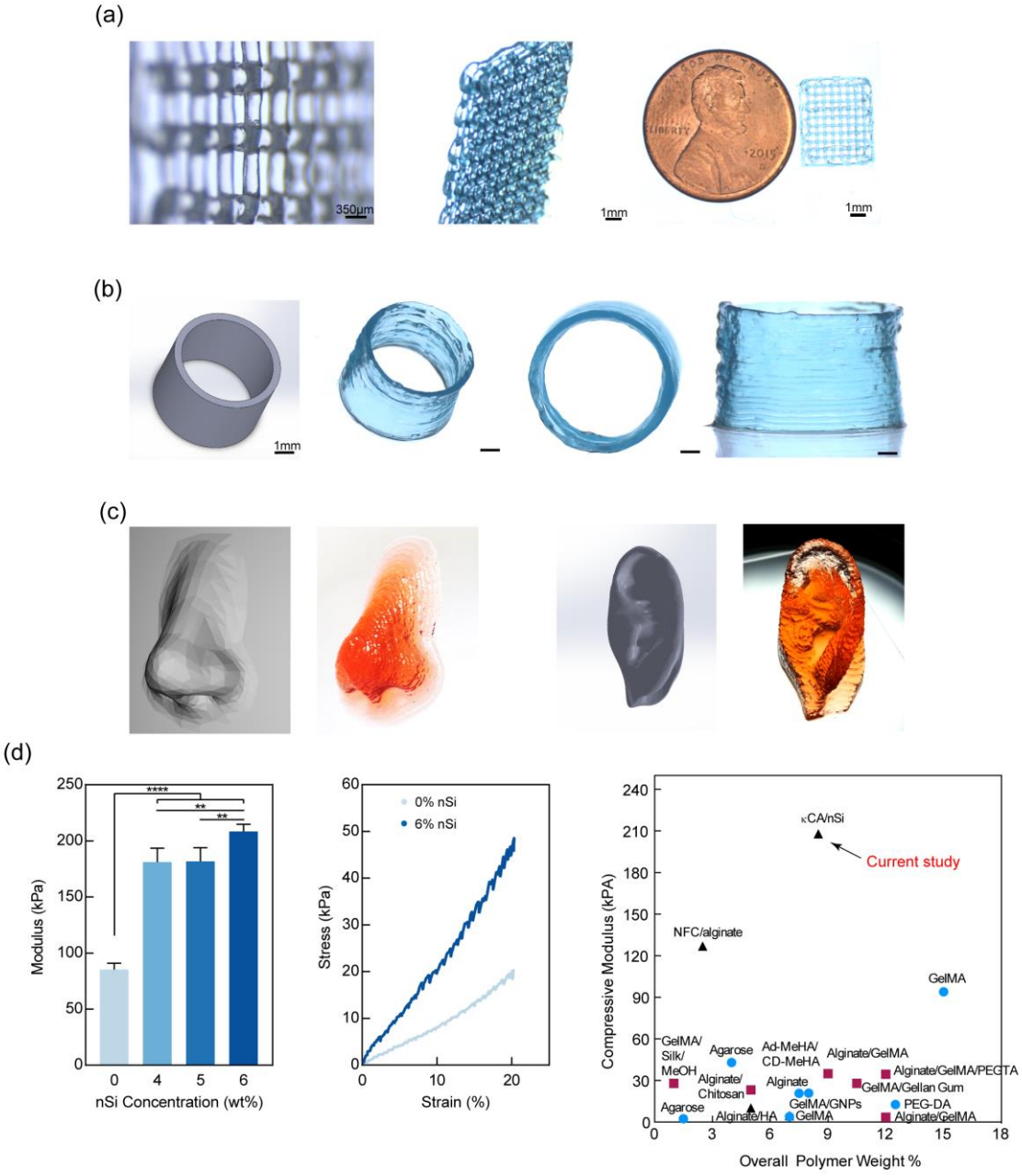

Figure 5: Evolution of printing complex structures with optimized κCA-nSi bioink. (a) κCA-nSi bioink is capable of printing complex constructs such as a single fiber in lattice network and 5 layered lattice network. (b) Printed 30 layer cylinder demonstrating bioinks' ability to print high aspect ratio constructs with high shape retention. (c) Printed anatomically relevant nose and ear with many layers, little deformation, and small over hangs. (d) Mechanical characterization of Mechanical characterization of κCA-nSi bioink. In comparison to currently available bioinks, the κCA-nSi bioink has a superior modulus.

3d Bioprinting Encapsulated Cells

Incorporation of cells into a bioink and ensuring their viability during printing is imperative to a successful bioink.[23] Due to the strong autofluorescence of the bioink and ability of nSi to adsorb fluorescent dyes, cells were stained with Cell Tracker green or red prior to loading into the bioink to visualize the distribution of cells within the printed structure (**Figure 6a and b**). Often the process of loading and mixing cells into viscous bioinks can be difficult, but due to the shear-thinning characteristics of κCA-nSi bioink, cells can be mixed with the bioink evenly without any cell aggregate or clamping. Finally, an Alamar Blue assay was performed to measure cell metabolic activity of encapsulated cells. The mean cell metabolic activity of the cells at day 1, 3 and 7 was similar and no significant difference was observed (**Figure 6c**). We believe the shear-thinning ability during printing and low yield stress during mixing provided a safe environment from shear-stress during the printing process. Other bioinks such as hyaluronic acid (HA)[8] and Alginate/nanocellulose[34] revealed similar cell survival on day 5 and 7.

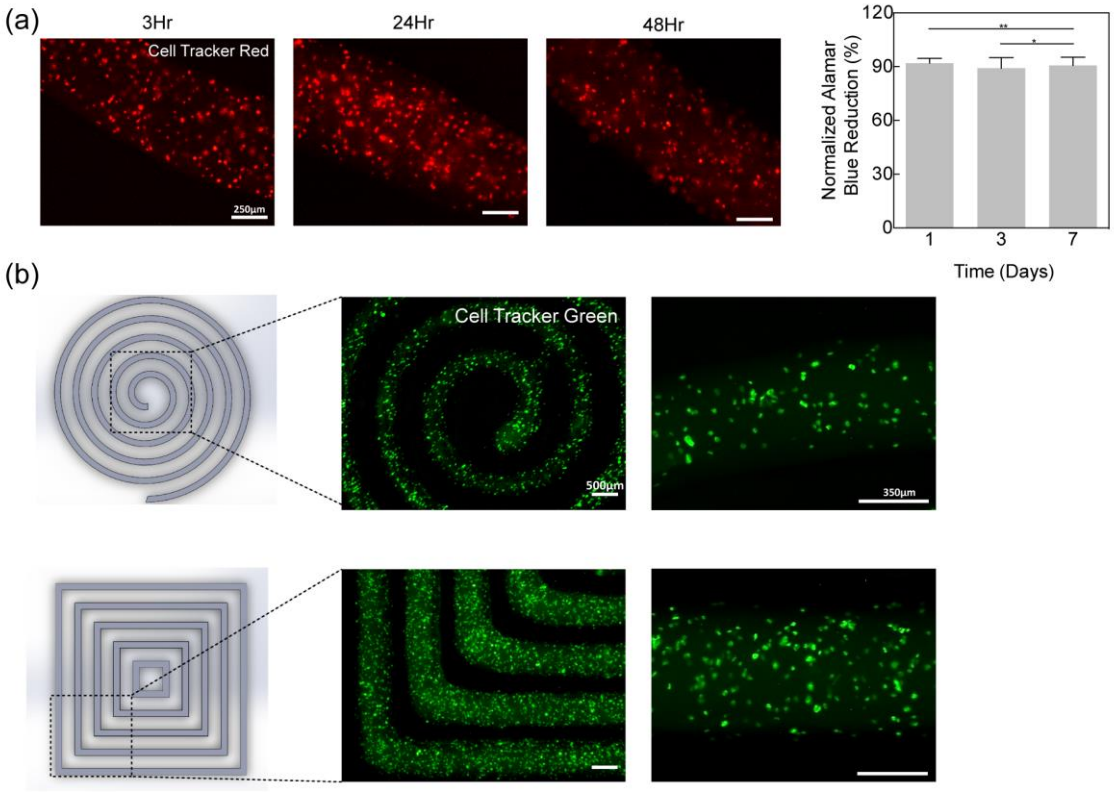

Figure 6: Bioprinted in vitro studies. (a) Fluorescent images using Cell Tracker Red showing cells evenly distributed in fibers immediately after 3, 24, and 48 hours. Alamar blue assay quantification demonstrating maintained metabolic activity, in printed constructs, for 1, 3, and 7 days. (c) Fluorescent images using Cell Tracker green revealing cell distribution in large patterned constructs.

CHAPTER IV

CONCLUSIONS

A rapidly gelling, self-supporting bioink from a natural polymer (κCA) reinforced with 2D nanoparticles (nanosilicate) is introduced. The κCA-nSi bioinks have shear-thinning characteristics and physiologically-relevant gelation temperatures. Strong interactions between κCA and nSi, results in enhanced physical interactions leading to high shape fidelity of printed filaments, and structural integrity of printed structures. After ionic crosslinking with K^+, κCA-nSi nanocomposites result in mechanical stiff hydrogels that could be used to print tissues which can sustain constant mechanical load, such as cartilage and blood vessels. Due to shear-thinning characteristics, high cell viability was observed in printed cells. In addition, the printed cells retained metabolic activity indicating the ability of κCA-nSi bioinks to support long-term cultures. Overall, κCA-nSi bioinks have high shape retention, structural fidelity, and mechanical strength that can be used to print complex physiologically relevant tissues.

REFERENCES

[1] M. Guvendiren, H.D. Lu, J.A. Burdick, Shear-thinning hydrogels for biomedical applications, Soft Matter 8(2) (2012) 260-272.

[2] W. Zhu, X. Ma, M. Gou, D. Mei, K. Zhang, S. Chen, 3D printing of functional biomaterials for tissue engineering, Current Opinion in Biotechnology 40 (2016) 103-112.

[3] S. Ahn, H. Lee, J. Puetzer, L.J. Bonassar, G. Kim, Fabrication of cell-laden three-dimensional alginate-scaffolds with an aerosol cross-linking process, Journal of Materials Chemistry 22(36) (2012) 18735-18740.

[4] A.G. Tabriz, M.A. Hermida, N.R. Leslie, W. Shu, Three-dimensional bioprinting of complex cell laden alginate hydrogel structures, Biofabrication 7(4) (2015) 045012.

[5] W. Schuurman, P.A. Levett, M.W. Pot, P.R. van Weeren, W.J.A. Dhert, D.W. Hutmacher, F.P.W. Melchels, T.J. Klein, J. Malda, Gelatin-Methacrylamide hydrogels as potential biomaterials for fabrication of tissue-engineered cartilage constructs, Macromolecular Bioscience 13(5) (2013) 551-561.

[6] L.E. Bertassoni, J.C. Cardoso, V. Manoharan, A.L. Cristino, N.S. Bhise, W.A. Araujo, P. Zorlutuna, N.E. Vrana, A.M. Ghaemmaghami, M.R. Dokmeci, A. Khademhosseini, Direct-write bioprinting of cell-laden methacrylated gelatin hydrogels, Biofabrication 6(2) (2014) 024105.

[7] L.A. Hockaday, K.H. Kang, N.W. Colangelo, P.Y. Cheung, B. Duan, E. Malone, J. Wu, L.N. Girardi, L.J. Bonassar, H. Lipson, C.C. Chu, J.T. Butcher, Rapid 3D printing

of anatomically accurate and mechanically heterogeneous aortic valve hydrogel scaffolds, Biofabrication 4(3) (2012) 035005.

[8] L. Ouyang, C.B. Highley, C.B. Rodell, W. Sun, J.A. Burdick, 3D printing of shear-thinning hyaluronic acid hydrogels with secondary cross-linking, ACS Biomaterials Science & Engineering (2016), 2 (10), pp 1743–1751

[9] C. De Maria, J. Rincon, A.A. Duarte, G. Vozzi, T. Boland, A new approach to fabricate agarose microstructures, Polymers for Advanced Technologies 24(10) (2013) 895-902.

[10] D.F. Duarte Campos, A. Blaeser, M. Weber, J. Jakel, S. Neuss, W. Jahnen-Dechent, H. Fischer, Three-dimensional printing of stem cell-laden hydrogels submerged in a hydrophobic high-density fluid, Biofabrication 5(1) (2013) 015003.

[11] W. Jia, P.S. Gungor-Ozkerim, Y.S. Zhang, K. Yue, K. Zhu, W. Liu, Q. Pi, B. Byambaa, M.R. Dokmeci, S.R. Shin, A. Khademhosseini, Direct 3D bioprinting of perfusable vascular constructs using a blend bioink, Biomaterials 106 (2016) 58-68.

[12] C. Colosi, S.R. Shin, V. Manoharan, S. Massa, M. Costantini, A. Barbetta, M.R. Dokmeci, M. Dentini, A. Khademhosseini, Microfluidic bioprinting of heterogeneous 3d tissue constructs using low-viscosity bioink, Advanced Materials 28(4) (2016) 677-684.

[13] F. Pati, J. Jang, D.-H. Ha, S. Won Kim, J.-W. Rhie, J.-H. Shim, D.-H. Kim, D.-W. Cho, Printing three-dimensional tissue analogues with decellularized extracellular matrix bioink, Nature Communications 5 (2014) 3935.

[14] F.P.W. Melchels, W.J.A. Dhert, D.W. Hutmacher, J. Malda, Development and characterisation of a new bioink for additive tissue manufacturing, Journal of Materials Chemistry B 2(16) (2014) 2282-2289.

[15] J.H. Chung, S. Naficy, Z. Yue, R. Kapsa, A. Quigley, S.E. Moulton, G.G. Wallace, Bio-ink properties and printability for extrusion printing living cells, Biomaterials Science 1(7) (2013) 763-773.

[16] D.B. Kolesky, K.A. Homan, M.A. Skylar-Scott, J.A. Lewis, Three-dimensional bioprinting of thick vascularized tissues, Proceedings of the National Academy of Sciences 113(12) (2016) 3179-3184.

[17] R.A. Barry, R.F. Shepherd, J.N. Hanson, R.G. Nuzzo, P. Wiltzius, J.A. Lewis, Direct-write assembly of 3d hydrogel scaffolds for guided cell growth, Advanced Materials 21(23) (2009) 2407-2410.

[18] H. Tekin, J.G. Sanchez, C. Landeros, K. Dubbin, R. Langer, A. Khademhosseini, Controlling spatial organization of multiple cell types in defined 3d geometries, Advanced Materials 24(41) (2012) 5543-5547.

[19] J. Jia, D.J. Richards, S. Pollard, Y. Tan, J. Rodriguez, R.P. Visconti, T.C. Trusk, M.J. Yost, H. Yao, R.R. Markwald, Y. Mei, Engineering alginate as bioink for bioprinting, Acta Biomater 10(10) (2014) 4323-31.

[20] Z. Wu, X. Su, Y. Xu, B. Kong, W. Sun, S. Mi, Bioprinting three-dimensional cell-laden tissue constructs with controllable degradation, Scientific Reports 6 (2016) 24474.

[21] B. Duan, State-of-the-art review of 3d bioprinting for cardiovascular tissue engineering, Annals of Biomedical Engineering (2016) 1-15.

[22] T. Billiet, M. Vandenhaute, J. Schelfhout, S. Van Vlierberghe, P. Dubruel, A review of trends and limitations in hydrogel-rapid prototyping for tissue engineering, Biomaterials 33(26) (2012) 6020-6041.

[23] I.T. Ozbolat, M. Hospodiuk, Current advances and future perspectives in extrusion-based bioprinting, Biomaterials 76 (2016) 321-343.

[24] L. Gasperini, J.F. Mano, R.L. Reis, Natural polymers for the microencapsulation of cells, Journal of the Royal Society Interface 11(100) (2014) 20140817.

[25] E.G. Popa, P.P. Carvalho, A.F. Dias, T.C. Santos, V.E. Santo, A.P. Marques, C.A. Viegas, I.R. Dias, M.E. Gomes, R.L. Reis, Evaluation of the in vitro and in vivo biocompatibility of carrageenan-based hydrogels, Journal of Biomedical Materials Research. Part A 102(11) (2014) 4087-97.

[26] K. Nishinari, M. Watase, Effects of sugars and polyols on the gel-sol transition of kappa-carrageenan gels, Thermochimica Acta 206 (1992) 149-162.

[27] A. Tecante, M. Núñez Santiago, J. De Vicente, Solution properties of κ-carrageenan and its interaction with other polysaccharides in aqueous media, InTech (2012), DOI: 10.5772/36619

[28] A.M. Hermansson, E. Eriksson, E. Jordansson, Effects of potassium, sodium and calcium on the microstructure and rheological behaviour of kappa-carrageenan gels, Carbohydrate Polymers 16(3) (1991) 297-320.

[29] P. Li, N.H. Kim, D. Hui, K.Y. Rhee, J.H. Lee, Improved mechanical and swelling behavior of the composite hydrogels prepared by ionic monomer and acid-activated Laponite, Applied Clay Science 46(4) (2009) 414-417.

[30] C.-W. Chang, A. van Spreeuwel, C. Zhang, S. Varghese, PEG/clay nanocomposite hydrogel: a mechanically robust tissue engineering scaffold, Soft Matter 6(20) (2010) 5157-5164.

[31] J.I. Dawson, R.O.C. Oreffo, Clay: New opportunities for tissue regeneration and biomaterial design, Advanced Materials 25(30) (2013) 4069-4086.

[32] S. Liu, W.L. Chan, L. Li, Rheological properties and scaling laws of κ-carrageenan in aqueous solution, Macromolecules 48(20) (2015) 7649-7657.

[33] A. Panwar, L.P. Tan, Current status of bioinks for micro-extrusion-based 3d bioprinting, Molecules (Basel, Switzerland) 21(6) (2016).

[34] K. Markstedt, A. Mantas, I. Tournier, H. Martínez Ávila, D. Hägg, P. Gatenholm, 3D bioprinting human chondrocytes with nanocellulose–alginate bioink for cartilage tissue engineering applications, Biomacromolecules 16(5) (2015) 1489-1496.

[35] Y. He, F. Yang, H. Zhao, Q. Gao, B. Xia, J. Fu, Research on the printability of hydrogels in 3D bioprinting, Scientific Reports 6 (2016) 29977.

[36] R.A. Rezende, P.J. Bártolo, A. Mendes, R.M. Filho, Rheological behavior of alginate solutions for biomanufacturing, Journal of Applied Polymer Science 113(6) (2009) 3866-3871.

[37] F. Belalia, N.-E. Djelali, Rheological properties of sodium alginate solutions, Rev Roum Chim 59 (2014) 135-145.

[38] A. Blaeser, D.F. Duarte Campos, U. Puster, W. Richtering, M.M. Stevens, H. Fischer, Controlling shear stress in 3d bioprinting is a key factor to balance printing resolution and stem cell integrity, Adv Healthc Mater 5(3) (2016) 326-33.

[39] K. Haraguchi, Synthesis and properties of soft nanocomposite materials with novel organic/inorganic network structures, Polym J 43(3) (2011) 223-241.

[40] K. Haraguchi, H.-J. Li, K. Matsuda, T. Takehisa, E. Elliott, Mechanism of forming organic/inorganic network structures during in-situ free-radical polymerization in pnipa−clay nanocomposite hydrogels, Macromolecules 38(8) (2005) 3482-3490.

[41] K. Haraguchi, R. Farnworth, A. Ohbayashi, T. Takehisa, Compositional effects on mechanical properties of nanocomposite hydrogels composed of poly(n,n-dimethylacrylamide) and clay, Macromolecules 36(15) (2003) 5732-5741.

[42] S.V. Murphy, A. Atala, 3D bioprinting of tissues and organs, Nat Biotech 32(8) (2014) 773-785.

[43] J. Radhakrishnan, A. Subramanian, U.M. Krishnan, S. Sethuraman, Injectable and 3D bioprinted polysaccharide hydrogels: from cartilage to osteochondral tissue engineering, Biomacromolecules 18(1) (2017) 1-26.

[44] C. Colosi, M. Costantini, R. Latini, S. Ciccarelli, A. Stampella, A. Barbetta, M. Massimi, L. Conti Devirgiliis, M. Dentini, Rapid prototyping of chitosan-coated alginate scaffolds through the use of a 3D fiber deposition technique, Journal of Materials Chemistry B 2(39) (2014) 6779-6791.

[45] W. Xiao, J. He, J.W. Nichol, L. Wang, C.B. Hutson, B. Wang, Y. Du, H. Fan, A. Khademhosseini, Synthesis and characterization of photocrosslinkable gelatin and silk fibroin interpenetrating polymer network hydrogels, Acta Biomaterialia 7(6) (2011) 2384-2393.

[46] G. Gao, A.F. Schilling, T. Yonezawa, J. Wang, G. Dai, X. Cui, Bioactive nanoparticles stimulate bone tissue formation in bioprinted three-dimensional scaffold and human mesenchymal stem cells, Biotechnology Journal 9(10) (2014) 1304-1311.

[47] K. Zhu, S.R. Shin, T. van Kempen, Y.-C. Li, V. Ponraj, A. Nasajpour, S. Mandla, N. Hu, X. Liu, J. Leijten, Y.-D. Lin, M.A. Hussain, Y.S. Zhang, A. Tamayol, A. Khademhosseini, Gold nanocomposite bioink for printing 3d cardiac constructs, Advanced Functional Materials 27(12) (2017) 1605352-n/a.